Letter

Diagnosing the origin and impact of low-mode asymmetries in ignition experiments at the National Ignition Facility

D. Casey [1],[*] B. MacGowan [1] O. Hurricane [1] O. Landen,[1] R. Nora [1] S. Haan,[1] A. Kritcher,[1]
A. Zylstra,[1] J. Ralph,[1] E. Dewald,[1] M. Hohenberger,[1] A. Pak,[1] P. Springer,[1] C. Weber,[1] J. Milovich,[1]
L. Divol,[1] E. Hartouni [1] R. Bionta,[1] K. Hahn,[1] D. Schlossberg,[1] A. Moore,[1] and M. Gatu Johnson [2]

[1]*Lawrence Livermore National Laboratory, Livermore, CA 94550, USA*

[2]*Massachusetts Institute of Technology (MIT), Cambridge, 02139 Massachusetts, USA*

Inertial confinement fusion ignition requires high inflight shell velocity, good energy coupling between the hotspot and shell, and high areal density at peak compression. Three-dimensional asymmetries caused by imperfections in the drive symmetry or target can grow and damage the coupling and confinement. Recent high-yield experiments have shown that low-mode asymmetries are a key degradation mechanism and contribute to variability. We show the experimental signatures and impacts of asymmetry change with increasing implosion yield given the same initial cause. This letter has implications for improving robustness to a key degradation in ignition experiments.

Lawson's criterion for ignition was exceeded [1] in inertial confinement fusion experiments at the National Ignition Facility (NIF) [2]. In these experiments, fuel-filled pellets are imploded to high densities and temperatures to initiate α-particle self-heating and fusion burn [3,4]. At the NIF, 192 laser beams irradiate the interior of a high-Z cylindrical hohlraum to indirectly drive the implosion with a nearly uniform, quasithermal, x-ray bath. The x-ray drive ablates the outer layers of the capsule, compressing the remaining ablator and an inner layer of cryogenically frozen DT radially inward. This imploding shell converges on and compresses a gaseous DT region to form a hotspot. For ignition to occur, the DT hotspot must have high enough energy density confined for adequate time to spark hotspot self-heating and start a burn wave through the dense DT shell. This requirement, shown by Lawson [5], can be expressed as a minimum value of $P\tau$, depending on the temperature (T), where P is the hotspot pressure and τ is the confinement time [6,7]. To produce high $P\tau$, an implosion must have high inflight implosion velocity (v_i), sufficient coupling between the inflight shell and hotspot, and high areal density (or ρR defined as $\rho R = \int \rho \, dr$) at stagnation.

The coupling of the shell kinetic energy and the confinement of that energy are degraded by three-dimensional (3D) ρR asymmetries. Recent analysis using a simplified two-piston system has shown [8] that many performance metrics can be expressed in terms of a parameter of asymmetry $f = \frac{\rho R_{\max} - \rho R_{\min}}{\rho R_{\max} + \rho R_{\min}} \approx \frac{v_{HS}}{v_i}$. Here, $\rho R_{\max}$ and $\rho R_{\min}$ are the maximum and minimum areal densities of the dense shell, respectively; v_{HS} is the bulk velocity of the burning hotspot near peak convergence, and v_i is the peak implosion velocity. In the limit of weak-α heating, the normalized residual kinetic energy nRKE $= f^2$, $\frac{P\tau}{P\tau_{1D}} \approx (1 - f^2)$ and $\frac{Y}{Y_{1D}} \approx (1 - f^2)^a$, where $\frac{Y}{Y_{1D}}$ is the yield (Y) normalized by idealized one-dimensional (1D) symmetric yield (Y_{1D}), and $a = 6$–$1.5 \, \ln(T)$ and accounts for the temperature (T in keV) dependence of the DT reactivity. This demonstrates ρR asymmetry is a primary degradation mechanism of ignition experiments.

Imperfections in radiation drive or target uniformity will seed asymmetries that grow during the implosion. Implosion experiments commonly exhibit signatures of significant asymmetry, and understanding their origin is of paramount importance. Herein, we show that the main sources of mode-1 asymmetry [9] in ignition experiments have been identified in ∼70% of cases and that their impact is in some cases significant (∼2× in yield) at yields >10^{17}. Importantly, having identified some principal causes of 3D asymmetries, we can attempt to reduce their origin and modify designs to be more robust to low-mode asymmetry.

Lawson's criteria was exceeded in NIF shot N210808, which produced 1.37 MJ of DT fusion energy [1,10,11] using a 6.40-mm-diameter depleted uranium (DU) hohlraum with a thin Au overcoat irradiated by 1.9 MJ of laser energy on target. Several repeat experiments have been performed to understand the variability near ignition and sensitivity to uncontrolled but diagnosable degradation mechanisms like $\ell = 1$ low-mode asymmetry. In these experiments, the laser beams enter through 3.1-mm-diameter laser entrance holes at each end of the cylindrical hohlraum. The hohlraum was filled with helium gas to 0.3 mg/cc to tamp the hohlraum wall. Inside the hohlraum is a 65-μm-thick cryogenically frozen deuterium-tritium ice layer of density 0.255 g/cm^3 inside a 1050 μm inner radius high-density carbon (HDC) [10–29] capsule. The capsules were 80-μm-thick HDC [28] doped with a small (∼0.4%) amount of W to help manage instability growth [30].
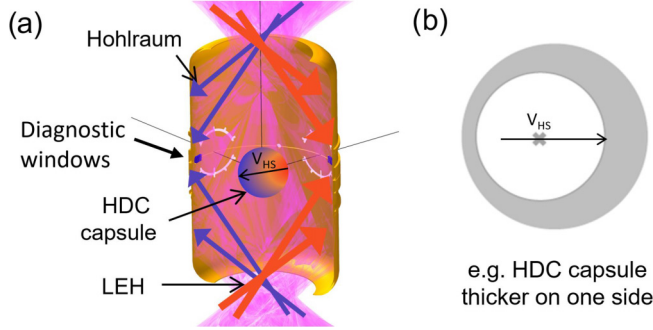
*casey21@llnl.gov

FIG. 1. Two main classes of $\ell = 1$ asymmetry seeds have been identified: (a) drive (laser and hohlraum penetrations, i.e., windows) and (b) capsule-ablator asymmetries.

Two key causes for $\ell = 1$ low-mode asymmetry have been uncovered in previous work [9]: drive asymmetries and capsule asymmetries. Drive asymmetries are known to be caused by laser mistiming, power imbalances [31], hohlraum dynamics, and hohlraum patches [9]. Capsule asymmetries are caused by thickness nonuniformity of the cryogenic DT layer [32], capsule thickness or mass [33], or nonuniformity of the ablation rate during the implosion [34] (illustrated in Fig. 1). Any of these asymmetries can manifest into significant distortions of the implosion at peak compression. For example, if the drive is $\sim 1\%$ weaker on the north pole of the capsule than the south pole, or equivalently, if the capsule has larger mass by $\sim 1\%$ on the north pole than the south pole, the south pole will accelerate to higher peak velocity. When the capsule begins decelerating, because the hotspot backpressure is nearly isobaric, both sides will begin to decelerate against similar pressures but at different radii. Ultimately, the lower-drive (or heavier) side will not converge as far and, because of spherical convergence, will have lower ρR and larger surface area contact against the hotspot, causing that side to bounce earlier and at larger radius. Internal hotspot flows are induced and flow outward toward the lower-ρR side at ~ 100 km/s. Radiation hydrodynamic simulations with the code HYDRA [35] confirm this qualitative description, as described by Spears *et al.* [36].

Here, v_{HS} is measured by observing the burn-averaged shift of the DT neutron emission with neutron spectroscopy [37–41]. However, at very high yield, tremendous pressure forces are produced affecting v_{HS}. Authors of previous studies of causes for v_{HS} have tended to treat it as directly proportional to the initial seed up to a point of saturation or as an output of integrated postshot simulations that somewhat obscure its physical meaning. However, simulations have shown [42] that, at a range of different performance levels, the proportionality of v_{HS} to seed is not fixed, an effect that requires spherical convergence to understand. The following analysis follows the approach of the asymmetric two-piston solution by Hurricane *et al.* [8] but extended to include spherical convergence and using a perturbed $\ell = 1$ Legendre p_1 interface such that $r(\theta) = p_0 + p_1 \cos(\theta)$.

Spherical convergence is critical to understanding how the $\ell = 1$ asymmetry grows during the implosion along with the influence of stagnation pressure and α heating. Therefore, a spherically convergent model is required to understand the relationship of stagnation asymmetries to initial seed and
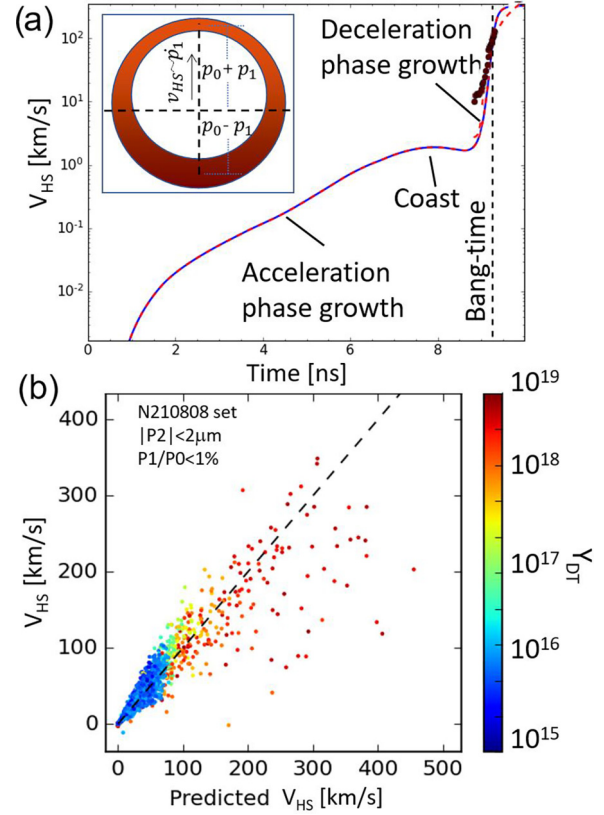

FIG. 2. (a) Simplified model of the implosion asymmetry in spherically convergent geometry. v_{HS} experiences explosive growth near peak convergence and burn during disassembly phase. (b) v_{HS} from HYDRA ensemble simulations plotted against the predicted v_{HS} from the simple analytic model where each point is colored by the total yield. The comparison shows general agreement on how v_{HS} changes for a given seed with increasing yield.

the response to increased pressure from α heating. During acceleration, and even more so during deceleration, linear growth transitions into nearly exponential growth because of convergent effects, as shown below.

Estimating the dynamic asymmetry, including the effects of hotspot backpressure and spherical convergence, begins by writing the equations of motion for p_0 and p_1 under the assumption that the pressure (P)-volume (V) relationship is $PV^\gamma \sim$ const. (valid for moderate levels of α heating, where α heating is comparable with radiation losses [8]; note that we will make a first-order extension for high levels of α heating subsequently). From Newton's law, the equations describing the Fig. 2(a) inset are

$$\ddot{p}_0 \pm \ddot{p}_1 = \frac{4\pi P_{PV}}{M} R_{PV}^5 \frac{(p_0 \pm p_1)^2}{\left(p_0^3 + 3p_1^2 p_0\right)^{5/3}}. \qquad (1)$$

Here, $\pm$ indicates the equations evaluated at either $\theta = 0(+)$ or $\theta = 180°(-)$, p_0 is the average shell radius (or r), p_1 is the amplitude of the asymmetry, and P_{PV} and R_{PV} are the pressure and radius at peak velocity, respectively. This model neglects lateral mass flow so that the mass in each solid angle element is preserved, and M is the mass that is in inertial contact with the hotspot or $M = cM_{shell}$, where $c \sim 0.67$ is

a correction on the initial shell mass (M_{shell}) for finite sound speed and compressibility expected to depend somewhat on shell adiabat (α). By first assuming that the perturbation to the volume is small, we can get an expression for the average radial trajectory:

$$\ddot{p}_0 = \frac{4\pi P_{\text{PV}}}{M} R_{\text{PV}}^5 \frac{1}{p_0^3}. \quad (2)$$

Like the solution of Ref. [43], a simplified solution is $p_0(t) \sim R_{\text{min}}\sqrt{1 + (t - t_{\text{min}})^2/\tau^2}$, where τ is the familiar inertial confinement time $\tau[\text{ns}]^{-1} \sim 1.12\sqrt{PR[\text{Gbar } \mu\text{m}]}/M[\text{ug}]$ [44–47], where P is the burn-averaged pressure and R is the burn-averaged radius. Now we can get an expression for p_1 in terms of p_0:

$$\ddot{p}_1 = 2\,p_1 \frac{\ddot{p}_0}{p_0}. \quad (3)$$

This relationship governs the growth of the asymmetry, which is sensitive to the shell acceleration $\ddot{p}_0$, the convergence $1/p_0$, and the asymmetry itself p_1. Here, v_{HS} is measured from a neutron-averaged quantity, sampling complicated profiles and flow fields [48] projected onto a detector array. Herein, we will assume v_{HS} is most sensitive to the overall implosion center-of-mass motion, and higher-order flows produce small corrections so that $v_{\text{HS}} \sim \dot{p}_1$, which will be tested against simulations. Figure 2(a) shows v_{HS} ($\dot{p}_1$) as a function of time with the various growth epochs called out. The asymmetry grows exponentially during both acceleration and deceleration, but the most extreme growth occurs during deceleration because that is when acceleration and convergence effects are largest. Note that p_1 and $\dot{p}_1$ have exact analytic solutions that can be written in terms of cosh, sinh, and $\tan^{-1}$; however, in this context, it is more illuminating to examine the expansion for $\dot{p}_1$ around minimum volume:

$$v_{\text{HS}} \sim \dot{p}_1 \sim \frac{p_{1\text{PV}}}{\tau}\cosh\left[\frac{\pi}{2}\right] + 2\frac{p_{1\text{PV}}}{\tau^2}\sinh\left[\frac{\pi}{2}\right](t - t_{\text{min}}).$$

This expression reveals that v_{HS} is sensitive to the asymmetry ($p_1\text{PV}$) at peak velocity, amplified by the inverse confinement time scale, which is related to peak acceleration at minimum volume ($\ddot{p}_0[R_{\text{min}}] = R_{\text{min}}\,\tau^{-2}$). The asymmetry at peak velocity can be estimated from a rocket model [33,49] as $p_1\text{PV} \sim \frac{1}{2}\frac{p_1}{p_0}R_i$, written in terms of the unimploded initial radius (R_i). Combining Eq. (3) at minimum volume with the estimate for $p_1\text{PV}$ and the earlier expression for τ results in

$$v_{\text{HS}} \sim \frac{1}{2}\frac{p_1}{p_0}R_i\cosh\left[\frac{\pi}{2}\right]1.12\sqrt{PR/M}. \quad (4)$$

Figure 2(b) shows the results of Eq. (4) compared with the x axis to ensemble simulations of N210808 on the y axis [50,51]. Equation (4) continues to match simulations with high yields, even when the underlying assumption $pV^\gamma =$ const. is violated. The reasons for this are subtle, as for very high-yield implosions, where thermonuclear energy increases faster than pdV expansion, cooling after the minimum volume, at least for a time. This means that the burn-weighted $\sqrt{PR/m}$ used to infer the acceleration is sampled after the minimum volume. Likewise, the period over which the asymmetry grows is longer because of the continuation of burn past

the minimum volume. To account for these effects, we can allow pV^γ to increase at the minimum volume, resulting in an effective time scale that accounts for the growth up to the minimum volume (τ_{mv}) and then the growth after and up to peak burn or bang time (τ_{BT}) using $\tau_{\text{eff}} = \sqrt{\tau_{\text{mv}}\tau_{\text{BT}}}$. Next, we can use the hotspot temperature equation [43,52] to estimate the time it takes for the expansion phase pdV cooling ($Q_{pdV} = -\frac{1}{m}p\frac{dV}{dt}$) to balance α-heating power (so $\frac{dT}{dt} \sim 0$) and hence begin to quench the thermonuclear burn. The α-heating term is $f_\alpha Q_\alpha = 8 \times 10^{24}\, f_\alpha \rho\langle\sigma v\rangle$. This can be rewritten by balancing the thermonuclear and confinement time scales [4,53] and introducing the burnup fraction $f_b \sim f_\alpha \rho\langle\sigma v\rangle\tau/m$ to become $f_\alpha Q_\alpha \sim \frac{34}{\tau}\frac{f_b}{1-f_b}$ in units of GJ s^{-1} g^{-1}. Solving for the time scale after the minimum volume ($\delta t = t - t_{\text{min}}$) when $Q_{pdV} \sim f_\alpha Q_\alpha$ results in $\frac{\delta t}{\tau} \sim \frac{150}{T}\frac{f_b}{1-f_b}$, where T is in units of keV. A similar argument can be made simply from the difference in acceleration time scales ($\sqrt{p_0/\ddot{p}_0}$) or reduction in confinement time between that at the minimum volume (τ_{mv}) and at bang time (τ_{BT}) so that $\delta t = \frac{1}{2}(\tau_{\text{mv}} - \tau_{\text{BT}})$ [54]. The result is $v_{\text{HS}} \sim \frac{p_1\text{PV}}{\tau_{\text{mv}}\tau_{\text{BT}}}\cosh[\frac{\pi}{2}] + 2\frac{p_1\text{PV}}{\tau_{\text{mv}}\tau_{\text{BT}}}\sinh[\frac{\pi}{2}]\delta t$. Using the fact that $\cosh[\frac{\pi}{2}]$ is the same order as $\sinh[\frac{\pi}{2}]$, $v_{\text{HS}} \sim \frac{1}{2}\frac{p_1}{p_0}R_i\frac{1}{\tau_{\text{BT}}}\cosh[\frac{\pi}{2}]$ reduces back to the form of Eq. (4), explaining why Eq. (4) continues to work at high yields. At yields $> 10^{18}$, the scatter between simulation and model increases. Recent work has shown that some of the scatter can be explained with increased numerical noise in simulating v_{HS} over the shorter time scale of high-yield burn. Nevertheless, there remains the possibility of additional burn-propagation-related physics that contribute also to this increased scatter, an area of active research [55].

The observed $\ell = 1$ asymmetry is diagnosed in magnitude and direction principally using v_{HS} measured with the high-precision fused silica nTOF diagnostic suite [41]. The measured hotspot velocity for N210808 and repeat experiments is shown in Fig. 3 in magnitude (grayscale) and direction using NIF chamber θ/φ coordinate plots. The initial seeds for $\ell = 1$ asymmetry are determined from a laser power balance view factor calculation and from the measured capsule mass asymmetry [9]. To compare the seeds with the measured v_{HS} directly, we first assume that the individual seeds can be combined in net vector addition following the procedure developed by MacGowan *et al.* [9]. Next, the sensitivity for each seed, including the effects of high yield, is estimated from Eq. (4) to produce a predicted hotspot velocity ($\overrightarrow{v_{\text{pred}}}$). It is worth noting that the hotspot velocity sensitivity is significantly enhanced at yields $> 10^{17}$ (up to $\sim 2\times$). A comparison between the measured hotspot velocity vector and the predicted hotspot velocity using Eq. (4) can be made by following the procedure described by MacGowan *et al.* [9] using the reduced χ^2 metric $\chi_\nu^2 = (\overrightarrow{v_{\text{HS}}} - \overrightarrow{v_{\text{pred}}})^T C^{-1}(\overrightarrow{v_{\text{HS}}} - \overrightarrow{v_{\text{pred}}})$, where C is the covariance of $(\overrightarrow{v_{\text{HS}}} - \overrightarrow{v_{\text{pred}}})$, including the effects of high yield using Eq. (4). This approach shows that 4 out 6 experiments or $\sim 67\%$ have $\chi_\nu^2 \sim 1$ [56], while only 2 out of 6 experiments or $\sim 33\%$ have $\chi_\nu^2 \sim 1$ without using Eq. (4) in the earlier approach of assuming static sensitivities. Therefore, this work is a critically important development in understanding the cause of $\ell = 1$ asymmetries in implosion at high yield.
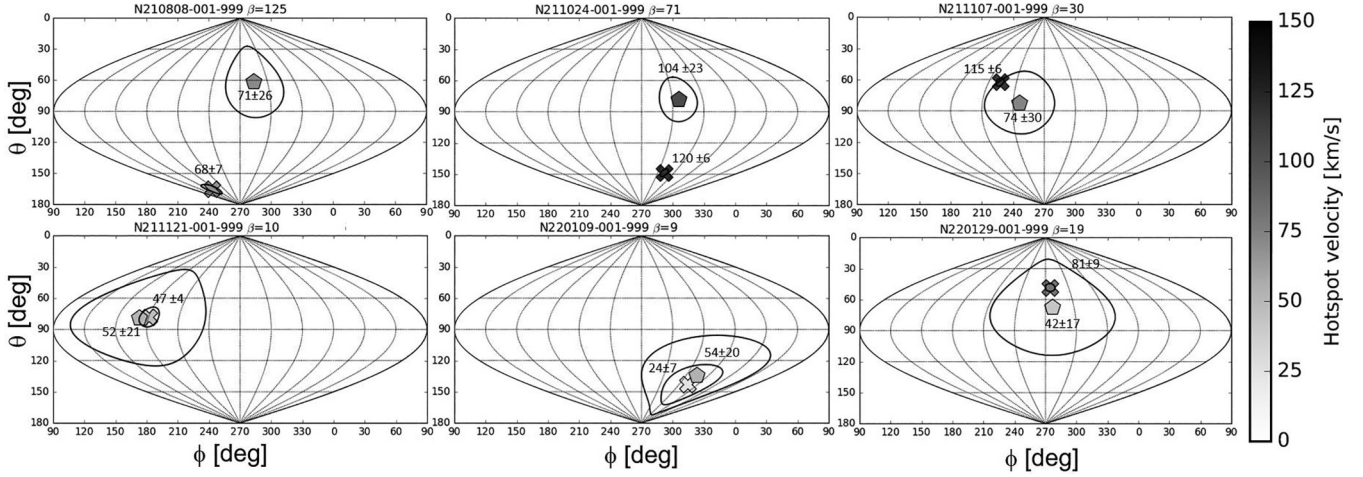
FIG. 3. Analysis of the net asymmetry from all known seeds for N210808 and repeat experiments (including the yield dependence of v_{HS} from Eq. (4) compared with the observed hotspot velocity (X symbol is measured, pentagon is predicted; in grayscale in km/s).

Just as important, however, this also shows that $\ell = 1$ asymmetry with the same seed will have a more significant degradation at higher yield than previous approaches have shown. This is shown by estimating impact beginning with a correction for α heating [8]:

$$\frac{Y}{Y_{1D}} \approx (1 - f^2)^a \exp[-1.2(a-1)\chi^{1.2}f^2], \quad (5)$$

where χ is the generalized Lawson criteria (GLC) [6,57] and f is evaluated using the α-on and degraded $f = v_{HS}/v_i$ [58,59] but now expressed in terms of the initial seed using Eq. (4):

$$f^2 = \mathrm{nRKE} = \left(\frac{p_1}{p_0}\right)^2 \frac{R_i^2}{M} \frac{PR}{v_i^2}. \quad (6)$$

Figure 4(a) shows the prediction of v_{HS} for a given initial p_1/p_0 seed from Eq. (4) compared with 2D HYDRA simulations with two sets of simulations, one with $Y_{1D} = 4\,\mathrm{MJ}$ (red circles) and another with $Y_{1D} = 0.1\,\mathrm{MJ}$ (gray squares). Likewise, Fig. 4(b) shows the yield-over-clean (YOC) from Eqs. (5) and (6) compared with 2D HYDRA simulations for both the $Y_{1D} = 4\mathrm{MJ}$ (red curve) and $Y_{1D} = 0.1\mathrm{MJ}$ (gray curve) cases [60]. These results show how critically important the effects of high yield are, as shown Fig. 2(b). Here, a 0.5% $\ell = 1$ asymmetry that would degrade the yield by $\sim 14\%$ for a 0.1 MJ implosion is shown to degrade a 4 MJ implosion yield by a catastrophic $\sim 50\%$. The disparity in impact is even more dramatic for initial seeds $> 0.5\%$. Physically, what Eq. (6) shows is that increased hotspot energies and pressures at higher yield increase the work lost to higher residual kinetic energies for a given mode-1 seed. For very high yields (e.g., greater than the 4 MJ example shown), this approach may break down as the implosion begins to burn a significant fraction of the assembled fuel. Understanding how the $\ell = 1$ asymmetry behaves at much higher yields and fuel burn-up will be the subject of future work.

Figure 4(c) shows the total DT yield as a function of measured v_{HS} for shot N210808 and the repeat experiments. Also shown in the figure is the prediction of Eq. (5) set to match the performance of N210808 at the observed hotspot velocity

of 75 ± 7 km/s. Interestingly, about half of the experiments shown lie near the piston-model curve, suggesting that their performance was significantly degraded (up to $2\times$) by the asymmetry characterized by v_{HS}. The experiments that lie further from the curve (N211121, N220109, and N220129) all
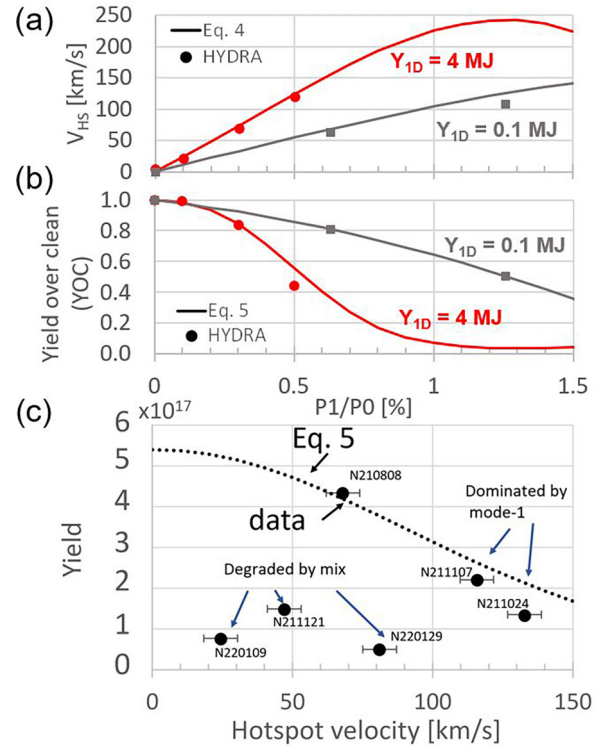

FIG. 4. (a) v_{HS} and (b) yield-over-clean (YOC) vs initial seed p_1/p_0 for the analytic model and two-dimensional (2D) HYDRA simulations for an implosion with a one-dimensional (1D) yield of 4 MJ (red) and an implosion with a 1D yield of 0.1 MJ (gray). (c) Plot of nTOF measured v_{HS} vs yield for N210808 and repeat experiments compared with the α-on piston model scaled to N210808. This analysis indicates that N211024 and N211107 were significantly degraded by $\ell = 1$ asymmetry and suggests that even N210808 suffered some degradation from 1D.
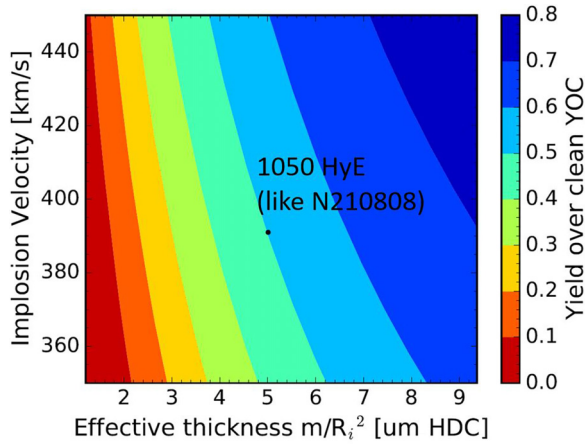
FIG. 5. Contours of yield-over-clean (YOC) subject to a seed $\ell = 1$ flux asymmetry that induces YOC = 0.5 at N210808-like initial conditions with a marginally igniting [generalized Lawson criteria (GLC) = 1] implosion plotted as function of effective shell thickness. Also shown is the operating point of N210808, which achieved 1.37 MJ and GLC $\sim PR/(420 \times 50) = 1.4$ [1]. The contours show the higher implosion velocity and/or with thicker effective shells are more robust to mode-1 asymmetry.

show strong indications of enhanced radiation losses in comparison between x-ray and neutron diagnostics, particularly imaging diagnostics. This has been attributed to the contamination of higher-Z HDC/W ablator materials into the hotspot from hydrodynamics instabilities or mix. Using a method like Pak *et al.* [61], $>0.5\,\mu g$ of localized ablator mix into the hotspot was estimated for N211121, N220109, and N220129, while the others show $< 0.25\,\mu g$ [62]. Therefore, about half of these experiments were dominated by $\ell = 1$ asymmetry and the other half by radiation loss induced by mix.

Interestingly, the analysis suggests that even N210808 was degraded $\sim 30\%$ by the observed $\ell = 1$ asymmetry [10,11]. That said, the seeds for N210808 are a poor match to v_{HS} for reasons that are not well understood, even if most of its repeat experiments can be explained. This could be because of undiagnosed changes (some $\sim 25\%$ of experiments historically remain anomalous with known seeds). It could also be related

to the very high pressures and gradients generated during burn propagation at yields $\gg 10^{17}$ enabling interactions of higher modes, pressure blowouts, or perhaps asymmetries in burn-propagation generating localized hydrodynamic blowout burnout. These hypotheses are under current investigation.

The experiments described herein provide a critically useful benchmark for the understanding of low-mode asymmetry at levels of α heating, and the models developed can suggest directions in implosion designs that are more resilient to asymmetries. In fact, Eq. (6) suggests an implosion that reaches equivalent GLC but, at smaller scale and/or with a heavier mass shell, could be more robust to initial perturbations of the same magnitude and origin. This is illustrated by Fig. 5. The figure shows the degradation or YOC estimated using Eqs. (5) and (6) for an implosion that marginally ignites as a function of the implosion velocity and the effective shell thickness (M/R_i^2), converted to units of μm of HDC assuming $\rho_{HDC} = 3.31\,g/cm^3$ for physical perspective.

In summary, the demonstration of ignition and propagating burn in the laboratory has enabled the study of $\ell = 1$ asymmetry in a an ignited plasma high-pressure regime. We have found using a model that v_{HS} changes at high yield in response to the higher pressures generated and because of burn propagation, a fact confirmed with simulations. Additionally, the performance degradation is shown to grow more virulent in the proximity of ignition, making the management of low-mode asymmetry even more critical toward achieving gains $\gg 1$. These developments have enabled a seed analysis that shows $\sim 67\%$ of the observations in this regime are explainable in terms of the known $\ell = 1$ seeds, consistent with historical trends [9]. Furthermore, low-mode asymmetry remains one of the dominant degradations in this igniting plasma regime, and the tools developed in this letter have shown that requirements on target and laser inducement seeds may need to be revised, while simultaneously revealing design directions that may be more robust to asymmetry if the seeds cannot be substantially improved.

[1] H. Abu-Shawareb, R. Acree, P. Adams, J. Adams, B. Addis, R. Aden, P. Adrian, B. B. Afeyan, M. Aggleton, L. Aghaian *et al.*, Phys. Rev. Lett. **129**, 075001 (2022).

[2] E. I. Moses, J. Phys. Conf. Ser. **112**, 012003 (2008).

[3] J. D. Lindl, P. Amendt, R. L. Berger, S. G. Glendinning, S. H. Glenzer, S. W. Haan, R. L. Kauffman, O. L. Landen, and L. J. Suter, Phys. Plasmas **11**, 339 (2004).

[4] S. Atzeni and J. Meyer-ter-Vehn, *The Physics of Inertial Fusion* (Oxford University Press, Oxford, 2004).

[5] J. D. Lawson, Proc. Phys. Soc. B **70**, 6 (1957).

[6] J. P. Freidberg, *Plasma Physics and Fusion Energy* (Cambridge University Press, Cambridge, 2007).

[7] R. Betti, P. Y. Chang, B. K. Spears, K. S. Anderson, J. Edwards, M. Fatenejad, J. D. Lindl, R. L. McCrory, R. Nora, and D. Shvarts, Phys. Plasmas **17**, 058102 (2010).

[8] O. A. Hurricane, D. T. Casey, O. Landen, A. L. Kritcher, R. Nora, P. K. Patel, J. A. Gaffney, K. D. Humbird, J. E. Field, M. K. G. Kruse *et al.*, Phys. Plasmas **27**, 062704 (2020).

[9] B. J. MacGowan, O. L. Landen, D. T. Casey, C. V. Young, D. A. Callahan, E. P. Hartouni, R. Hatarik, M. Hohenberger, T. Ma, D. Mariscal *et al.*, High Energy Density Phys. **40**, 100944 (2021).

[10] A. L. Kritcher, A. B. Zylstra, D. A. Callahan, O. A. Hurricane, C. R. Weber, D. S. Clark, C. V. Young, J. E. Ralph, D. T. Casey, A. Pak *et al.*, Phys. Rev. E **106**, 025201 (2022).

[11] A. B. Zylstra, A. L. Kritcher, O. A. Hurricane, D. A. Callahan, J. E. Ralph, D. T. Casey, A. Pak, O. L. Landen, B. Bachmann, K. L. Baker *et al.*, Phys. Rev. E **106**, 025202 (2022).

[12] D. D. Ho, Bull. Am. Phys. Soc. **52**, 273 (2007).

[13] A. J. MacKinnon, N. B. Meezan, J. S. Ross, S. Le Pape, L. Berzak Hopkins, L. Divol, D. Ho, J. Milovich, A. Pak, J. Ralph *et al.*, Phys. Plasmas **21**, 056318 (2014).

[14] J. S. Ross, D. Ho, J. Milovich, T. Doppner, J. McNaney, A. G. MacPhee, A. Hamza, J. Biener, H. F. Robey, E. L. Dewald *et al.*, Phys. Rev. E **91**, 021101(R) (2015).

[15] L. F. Berzak Hopkins, N. B. Meezan, S. Le Pape, L. Divol, A. J. Mackinnon, D. D. Ho, M. Hohenberger, O. S. Jones, G. Kyrala, J. L. Milovich *et al.*, Phys. Rev. Lett. **114**, 175001 (2015).

[16] D. D. M. Ho, S. W. Haan, J. D. Salmonson, D. S. Clark, J. D. Lindl, J. L. Milovich, C. A. Thomas, L. F. B. Hopkins, and N. B. Meezan, J. Phys. Conf. Ser. **717**, 012023 (2016).

[17] N. B. Meezan, L. F. Berzak Hopkins, S. Le Pape, L. Divol, A. J. MacKinnon, T. Döppner, D. D. Ho, O. S. Jones, S. F. Khan, T. Ma *et al.*, Phys. Plasmas **22**, 062703 (2015).

[18] L. Divol, A. Pak, L. F. Berzak Hopkins, S. Le Pape, N. B. Meezan, E. L. Dewald, D. D.-M. Ho, S. F. Khan, A. J. Mackinnon, J. S. Ross *et al.*, Phys. Plasmas **24**, 056309 (2017).

[19] L. F. Berzak Hopkins, S. Le Pape, L. Divol, N. B. Meezan, A. J. Mackinnon, D. D. Ho, O. S. Jones, S. Khan, J. L. Milovich, J. S. Ross *et al.*, Phys. Plasmas **22**, 056318 (2015).

[20] A. L. Kritcher, D. Clark, S. Haan, S. A. Yi, A. B. Zylstra, D. A. Callahan, D. E. Hinkel, L. F. Berzak Hopkins, O. A. Hurricane, O. L. Landen *et al.*, Phys. Plasmas **25**, 056309 (2018).

[21] H. F. Robey, L. Berzak Hopkins, J. L. Milovich, and N. B. Meezan, Phys. Plasmas **25**, 012711 (2018).

[22] D. T. Casey, C. A. Thomas, K. L. Baker, B. K. Spears, M. Hohenberger, S. F. Khan, R. C. Nora, C. R. Weber, D. T. Woods, O. A. Hurricane *et al.*, Phys. Plasmas **25**, 056308 (2018).

[23] K. L. Baker, C. A. Thomas, D. T. Casey, S. Khan, B. K. Spears, R. Nora, T. Woods, J. L. Milovich, R. L. Berger, D. Strozzi *et al.*, Phys. Rev. Lett. **121**, 135001 (2018).

[24] A. L. Kritcher, D. T. Casey, C. A. Thomas, A. B. Zylstra, M. Hohenberger, K. Baker, S. Le Pape, B. Bachmann, S. Bhandarkar, J. Biener *et al.*, Phys. Plasmas **27**, 052710 (2020).

[25] A. B. Zylstra, O. A. Hurricane, D. A. Callahan, A. L. Kritcher, J. E. Ralph, H. F. Robey, J. S. Ross, C. V. Young, K. L. Baker, D. T. Casey *et al.*, Nature (London) **601**, 542 (2022).

[26] A. L. Kritcher, C. V. Young, H. F. Robey, C. R. Weber, A. B. Zylstra, O. A. Hurricane, D. A. Callahan, J. E. Ralph, J. S. Ross, K. L. Baker *et al.*, Nat. Phys. **18**, 251 (2022).

[27] D. S. Clark, D. T. Casey, C. R. Weber, O. S. Jones, K. L. Baker, E. L. Dewald, L. Divol, A. Do, A. L. Kritcher, O. L. Landen *et al.*, Phys. Plasmas **29**, 052710 (2022).

[28] T. Braun, S. O. Kucheyev, S. J. Shin, Y. M. Wang, J. Ye, N. E. Teslich Jr., C. K. Saw, D. B. Bober, E. M. Sedillo, N. G. Rice *et al.*, Nucl. Fusion. **63**, 016022 (2023).

[29] M. Hohenberger, D. T. Casey, A. L. Kritcher, A. Pak, A. B. Zylstra, C. A. Thomas, K. L. Baker, S. Le Pape, B. Bachmann, R. L. Berger *et al.*, Phys. Plasmas **27**, 112704 (2020).

[30] D. S. Clark, J. L. Milovich, D. E. Hinkel, J. D. Salmonson, J. L. Peterson, L. F. Berzak Hopkins, D. C. Eder, S. W. Haan, O. S. Jones, M. M. Marinak *et al.*, Phys. Plasmas **21**, 112705 (2014).

[31] C. V. Young, L. Masse, D. T. Casey, B. J. MacGowan, O. L. Landen, D. A. Callahan, N. B. Meezan, R. Nora, and P. K. Patel, Phys. Plasmas **27**, 082702 (2020).

[32] S. W. Haan, J. Atherton, D. S. Clark, B. A. Hammel, D. A. Callahan, C. J. Cerjan, E. L. Dewald, S. Dixit, M. J. Edwards, S. Glenzer *et al.*, Fus. Sci. Tech. **63**, 67 (2013).

[33] D. T. Casey, B. J. MacGowan, J. D. Sater, A. B. Zylstra, O. L. Landen, J. Milovich, O. A. Hurricane, A. L. Kritcher, M. Hohenberger, K. Baker *et al.*, Phys. Rev. Lett. **126**, 025002 (2021).

[34] J. L. Milovich, D. C. Casey, B. MacGowan, D. Clark, D. Mariscal, T. Ma, K. Baker, R. Bionta, K. Hahn, A. Moore *et al.*, Plasma Phys. Controlled Fusion **63**, 025012 (2020).

[35] M. M. Marinak, G. D. Kerbel, N. A. Gentile, O. Jones, D. Munro, S. Pollaine, T. R. Dittrich, and S. W. Haan, Phys. Plasmas **8**, 2275 (2001).

[36] B. K. Spears, M. J. Edwards, S. Hatchett, J. Kilkenny, J. Knauer, A. Kritcher, J. Lindl, D. Munro, P. Patel, H. F. Robey *et al.*, Phys. Plasmas **21**, 042702 (2014).

[37] M. Gatu Johnson, J. P. Knauer, C. J. Cerjan, M. J. Eckart, G. P. Grim, E. P. Hartouni, R. Hatarik, J. D. Kilkenny, D. H. Munro, D. B. Sayre *et al.*, Phys. Rev. E **94**, 021202(R) (2016).

[38] R. Hatarik, D. B. Sayre, J. A. Caggiano, T. Phillips, M. J. Eckart, E. J. Bond, C. Cerjan, G. P. Grim, E. P. Hartouni, J. P. Knauer *et al.*, J. Appl. Phys. **118**, 184502 (2015).

[39] D. J. Schlossberg, G. P. Grim, D. T. Casey, A. S. Moore, R. Nora, B. Bachmann, L. R. Benedetti, R. M. Bionta, M. J. Eckart, J. E. Field *et al.*, Phys. Rev. Lett. **127**, 125001 (2021).

[40] H. G. Rinderknecht, D. T. Casey, R. Hatarik, R. M. Bionta, B. J. MacGowan, P. Patel, O. L. Landen, E. P. Hartouni, and O. A. Hurricane, Phys. Rev. Lett. **124**, 145002 (2020).

[41] A. S. Moore *et al.*, Rev. Sci. Instrum. **89**, 10I120 (2018).

[42] R. C. Nora *et al.*, Phys. Plasmas **30**, 092705 (2023).

[43] O. A. Hurricane, D. A. Callahan, D. T. Casey, E. L. Dewald, T. R. Dittrich, T. Döppner, S. Haan, D. E. Hinkel, L. F. Berzak Hopkins, O. Jones *et al.*, Nat. Phys. **12**, 800 (2016).

[44] Note, the product of *PR* (including α heating) can be inferred from the Ignition Threshold Factor (ITFX) using PR_a [Gbar μm] $= 8400 \times \text{ITFX}_a^{0.34} + 109 \times \text{ITFX}_a^{1.19}$ using a similar procedure as Patel [46] and Lindl [47].

[45] $\text{ITFX}_a = (\text{YDT}/4.0 \times 10^{15}) \times (173/M_{\text{shell}}[\text{ug}]) \times (\text{DSR}/0.067)^{2.1}$.

[46] P. K. Patel, P. T. Springer, C. R. Weber, L. C. Jarrott, O. A. Hurricane, B. Bachmann, K. L. Baker, L. F. Berzak Hopkins, D. A. Callahan, D. T. Casey *et al.*, Phys. Plasmas **27**, 13 (2020).

[47] J. D. Lindl, S. W. Haan, O. L. Landen, A. R. Christopherson, and R. Betti, Phys. Plasmas **25**, 122704 (2018).

[48] D. H. Munro, Nucl. Fusion **56**, 036001 (2016).

[49] O. A. Hurricane, A. Kritcher, D. A. Callahan, O. Landen, P. K. Patel, P. T. Springer, D. T. Casey, E. L. Dewald, T. R. Dittrich, T. Döppner *et al.*, Phys. Plasmas **24**, 092706 (2017).

[50] To remove the effects of mode-coupling and saturation, this comparison is filtered for simulations with primary neutron image $|p_2| < 2$ μm and applied $p_1/p_0 < 1\%$.

[51] In each capsule-only ensemble simulation, the seed p_1/p_0 asymmetry, the drive foot length, drive peak, and coast time (time between peak drive and bang time), the amount of preheat introduced into the ice, the amount of ice/ablator mix, and a multiplier on the drive mband spectrum (> 2 keV) were varied. In this set, the p_2/p_0 was also varied, but only simulations that were near round were used.

[52] P. T. Springer, O. A. Hurricane, J. H. Hammer, R. Betti, D. A. Callahan, E. M. Campbell, D. T. Casey, C. J. Cerjan, D. Cao, E. Dewald *et al.*, Nucl. Fusion **59**, 032009 (2019).

[53] G. S. Fraley, E. J. Linnebur, R. J. Mason, and R. L. Morse, The Physics of Fluids **17**, 474 (1974).

[54] The two prior expressions suggest a relationship between the reduction in the confinement and the burn-up fraction that HYDRA ensemble simulations confirm.

[55] R. Nora, private communication.

[56] Interestingly, the χ^2 distribution in these experiments shows two populations, one clustered ~ 1, indicating that the known target and laser inducements can explain the observation, and the other ~ 6, indicating outliers not well explained by the known seeds. We therefore use reduced $\chi^2 < 2$ to separate the two populations and quote the percentages of each.

[57] R. Betti, A. R. Christopherson, B. K. Spears, R. Nora, A. Bose, J. Howard, K. M. Woo, M. J. Edwards, and J. Sanz, Phys. Rev. Lett. **114**, 255003 (2015).

[58] O. A. Hurricane, D. T. Casey, O. Landen, D. A. Callahan, R. Bionta, S. Haan, A. L. Kritcher, R. Nora, P. K. Patel, P. T. Springer *et al.*, Phys. Plasmas **29**, 012703 (2022).

[59] Note that it has been shown also that $f^2 = 1 - \rho R_{\mathrm{WHM}}/\rho R_{\mathrm{avg}}$, where ρR_{WHM} is the weighted harmonic mean areal density and ρR_{avg} is the average areal density, a finding with implication on higher modes that will be explored in future work.

[60] To estimate the α-on degradation, several practical choices were made to compare with experiment. First, the degraded χ was used inferred directly from the measured data, and second, the degraded a was used from the measured T. Recall, the parameter $a = 6 - 1.5 \ln(T)$ for DT between 1 and 10 keV. This differs from the approach proposed in Hurricane *et al.* (2020) [8] based on undegraded 1D quantities for χ_{1D} and a_{1D}, but the result is numerically the same when degraded because of their nearly cancelling temperature dependence.

[61] A. Pak, L. Divol, C. R. Weber, L. F. Berzak Hopkins, D. S. Clark, E. L. Dewald, D. N. Fittinghoff, V. Geppert-Kleinrath, M. Hohenberger, S. Le Pape *et al.*, Phys. Rev. Lett. **124**, 145001 (2020).

[62] L. Divol *et al.*, private communication.